Double Transition Metal MXenes: Atomistic Design of Two-dimensional Carbides and Nitrides

Weichen Hong, Brian Wyatt, Srinivasa Kartik Nemani, and Babak Anasori

MXenes are a large family of two-dimensional (2D) transition metal carbides, nitrides, and carbonitrides. The MXene family has expanded since their discovery in 2011 and grew larger with the discovery of ordered double transition metal (DTM) MXenes. These DTM MXenes differ from their counterpart mono-transition metal (mono-M) MXenes, where two transition metals can occupy the metal sites. Ordered DTM MXenes are comprised of transition metals in either an in-plane or out-of-plane structure. Additionally, some DTM MXenes are in the form of solid solutions, which are defined by two randomly distributed transition metals throughout the 2D structure. MXenes different structures and array of transition metal pairs provide the ability to tune DTM MXenes for specific optical, magnetic, electrochemical, thermoelectric, catalytic, or mechanical behavior. This degree of control over their composition and structure is unique in the field of 2D materials and offers a new avenue for application-driven design of functional nanomaterials. In this review, we present the synthesis, structure, and properties of DTM MXenes and provide an outlook for future research in this field.

Introduction

Since 2004, there has been significant interest in the design of two-dimensional (2D) materials to meet rapidly evolving demands for advanced materials in technological applications, which ranges from energy storage,[1-3] electronics,[4] membranes,[5, 6] catalysts,[7] and sensors.[8, 9] MXenes are a large family of 2D materials, discovered in 2011,[10, 11] which offer a unique combination of electronic,[12-14] optical,[15-17] mechanical,[18-20] and colloidal properties.[21, 22] MXenes have high metallic conductivity (up to 15,100 $S \cdot cm^{-1}$ in $Ti_3C_2T_x$ film form),[23] are optically transparent (absorbing 3% of visible light/nm thickness),[17] exhibit a high modulus of elasticity (330-400 GPa),[18-20] and are electromagnetic interference shields [24] and electrochemically active materials.[25] MXenes are few-atom-thick 2D sheets with a general formula of $M_{n+1}X_nT_x$. In each MXene flake, $n + 1$ (n=1-4) layers of a transition metal (M) are interleaved with n layers of carbon or nitrogen (X).[25, 26] The T_x in the formula represents surface terminations, including =O, –OH, –F, and –Cl, which are bonded to the outer M layers.[25, 27, 28]

MXenes synthesis is a top-down approach by selectively etching the A-layers from three-dimensional (3D) crystalline layered carbides and nitrides,[29, 30] mostly MAX phases. In a MAX phase, $M_{n+1}X_n$ layers are bonded with an atomic layer of an A-group element, which is usually a group 13 to 16 element (Al, Ga, Si, Ge, P, As, etc.).[31] Three types of MAX phase structures, M_2AX, M_3AX_2, and M_4AX_3, are shown in Figure 1a. MAX phases are usually synthesized by reactive sintering of their elemental powder in stochiometric ratios, such as 3M:1A:2C for M_3AC_2, at temperatures above 1300 ºC under controlled atmosphere.[31] The M-A bonds are primary bonds, which makes mechanical exfoliation challenging. However, the M-A

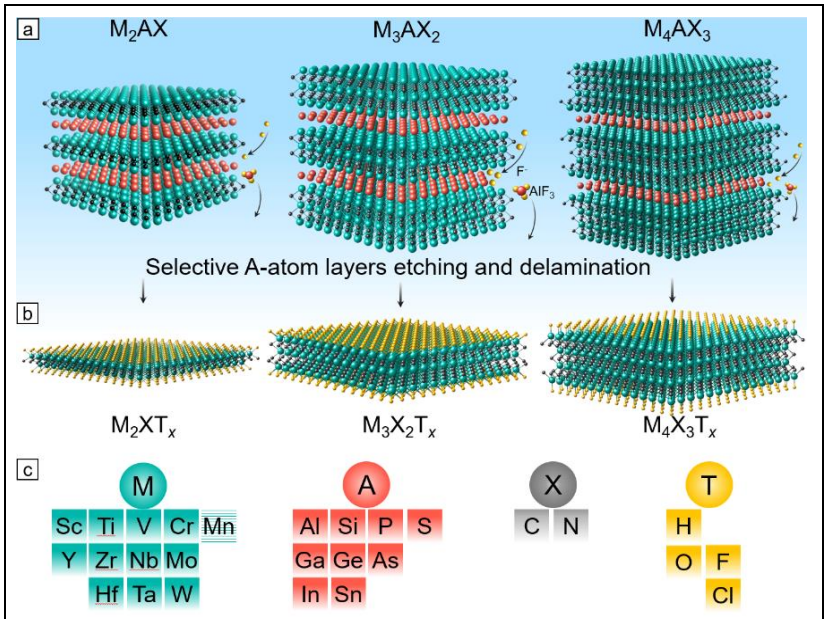

Figure 1. MXenes precursors and their synthesis. (a) Three types of mono-M MAX phases M_2AX, M_3AX_2, M_4AX_3 and the selective etching process of the A-group layers (red atoms). (b) MXenes are formed after the selective etching process and formation of surface terminations (yellow atoms) labeled as T. (c) Possible elements for M, A, X, and T in MAX and MXene phases. Mn exists in M sites in MAX phases, but Mn-containing MXenes are not yet synthesized, as denoted by the horizontal patterned background of Mn.

Weichen Hong12†, Brian Wyatt1†, Srinivasa Kartik Nemani1†, Babak Anasori1*
1Department of Mechanical and Engineering, and Integrated Nanosystems Development Institute, Purdue School of Engineering and Technology, Indiana University-Purdue University, Indianapolis, 46202, USA
2Department of Mechanical Engineering, Purdue University West Lafayette, 47907, USA
†These authors have contributed equally to this work.
*Corresponding author: banasori@iupui.edu

bonds are weaker in comparison to M-X bonds, which allows selective chemical etching of the A elements without disruption of the M-X bonds.[32] This consequently permits $M_{n+1}X_n$ layers to be readily delaminated.[10, 32] After selective removal of the A-group layers, transition metals in $M_{n+1}X_n$ are exposed. After exposure, M-elements become terminated with surface functional groups (T_x), which forms the chemical formula $M_{n+1}X_nT_x$ (Figure 1b). The composition of surface terminations is determined by the chemistry of the environment during etching,[33-35] the nature of M transition metal,[33] and post treatment methods.[36] The complete list of elements for M, X, T, and some of the A-group elements of MAX phases are shown in Figure 1c. The full list of A-group elements of MAX phases can be found elsewhere.[28, 31] Due to MXenes' top-down synthesis approach, the $M_{n+1}X_n$ composition is derived by the composition of their MAX phase precursors, as shown in Figure 1a and 1b.

MXenes can be classified into two separate categories based on their transition metal composition. First type is mono-transition metal (mono-M) MXenes (Figure 1), where M layers are made of a transition metal such as Ti_2CT_x, V_2CT_x, $Ti_3C_2T_x$, $Nb_4C_3T_x$.[28] Although there are many possible combinations of transition metals and carbon/nitrogen, only fourteen mono-M MXenes have been synthesized.[28] A second type of MXenes is known as double transition metal (DTM) MXenes (Figure 2). DTM MXenes are comprised of two distinct transition metals, differentiated by M′ and M″, where we indicate their atomic positions with green and purple, respectively, in Figure 2 and throughout this paper. DTM MXenes are further classified by structure into ordered[37, 38] (Figure 2a and 2b) and solid solution MXenes (Figure 2c).[39, 40] In ordered MXenes, the two different transition metals (M′ and M″) occupy the M layers in specific sites, defined as in-plane order (such as $Mo_{4/3}Y_{2/3}CT_x$[38]) or out-of-plane order (such as $Mo_2TiC_2T_x$[37, 41] and $Mo_2Ti_2C_3T_x$[37]).

In-plane ordered MXenes, defined by the formula $M'_{4/3}M''_{2/3}XT_x$, are comprised of two different transition metals ordered with alternating sites in each M-layer atomic plane (Figure 2a). Out-of-plane MXenes, defined by the formula $M'_2M''X_2T_x$ or $M'_2M''_2X_3T_x$, are comprised of ordered transition metals in separate atomic planes, where inner layers of M″ transition metals are sandwiched by outer layers of M′ transition metals (Figure 2b). In contrast to ordered MXenes, solid solution MXenes, defined by the formula $(M',M'')_{n+1}C_nT_x$, are comprised of two different transition metals randomly distributed in all M layers, such as $(Ti,V)_2CT_x$, $(Ti,Nb)_3C_2T_x$, and $(Nb,Zr)_4C_3T_x$ (Figure 2c). To date, all experimentally synthesized and theoretically predicted DTM MXenes are carbides, no DTM MXene nitrides or carbonitrides have been explored. Since the layered structures of DTM MXenes are derived from their parent MAX phases, it is the composition of the MAX phases that governs the composition of DTM MXenes. While more than twenty DTM MXenes have been

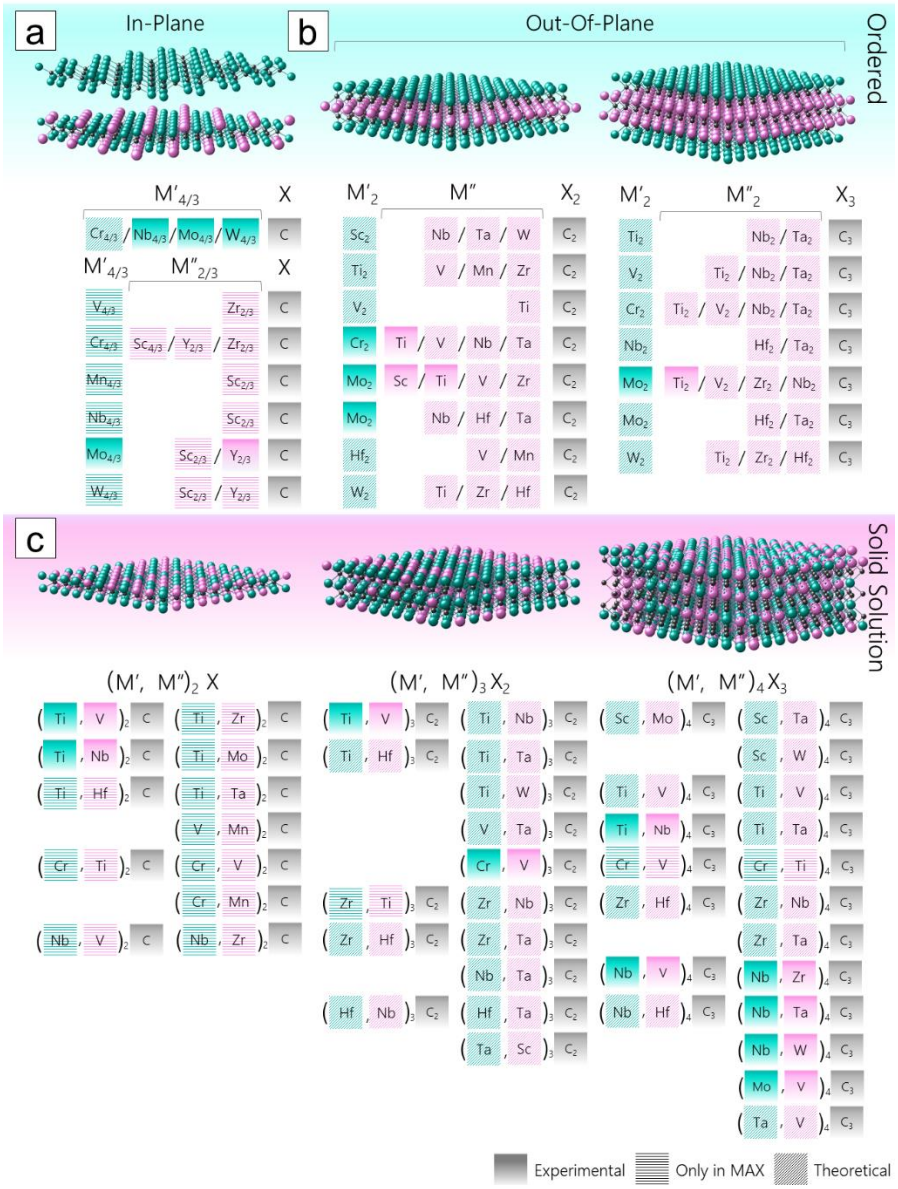

Figure 2. Experimental and theoretical DTM M_2X, M_3X_2, and M_4X_3 MXenes. The green and purple elements correspond to M′ and M″ transition metals, respectively. (a) In-plane order ($M'_{4/3}M''_{2/3}X$ shown in bottom) and in-plane divacancy order ($M'_{4/3}X$ shown in top). (b) Out-of-plane order ($M'_2M''X_2$ and $M'_2M''_2X_3$). (c) Solid solution MXenes are disordered, with M' and M" transition metals occupying random sites. M elements with solid gradient background refer to experimentally synthesized MXenes, while M elements with diagonal striped background represents MXenes explored by first principles studies and are yet to be synthesized. M elements with horizontal striped represent experimentally realized MAX phase precursors, but have not been etched to MXenes yet. In this figure, surface terminations (T_x: =O, –OH, –F, and –Cl) are not shown for simplicity.

synthesized from their precursor MAX (Figure 2, highlighted with a solid gradient background), there are many synthesized DTM MAX phases which have not yet been selectively etched to their corresponding DTM MXenes (Figure 2, highlighted with horizontal lines in the background). Similarly, there are additional theoretically predicted DTM MXenes which have not yet been experimentally realized in MXene or their DTM MAX phase precursor (Figure 2, highlighted with diagonal striped lines in the background).

DTM MXenes add many new compositions to the MXene family, with at least fifty ordered (Figure 2),[37, 42, 43] and a limitless number of solid solution MXenes.[39, 40, 44, 45] The possibility of control of the arrangement of transition metal atoms to form in-plane ordered, out-of-plane ordered, and solid solution DTM MXenes gives control over MXenes' electronic, magnetic, electrochemical, optical, and mechanical properties, which is unique to the field of 2D materials. To date, there is no direct transition from the mono-M MXenes to DTM ones, and the synthesis of DTM MXenes is possible only by selective topochemical etching of their DTM MAX phase precursors. This review aims to provide insight into DTM MXenes in terms of their unique structures, formation mechanisms, and subsequent tunable properties. We also provide insight toward future applications and necessary research in this growing field.

In-plane ordered double transition metal MXenes

In-plane ordered DTM MXenes are represented as $M'_{4/3}M''_{2/3}XT_x$ and are one of the latest additions to the MXene family.[38, 46] In-plane order is only observed in the thinnest MXene structure, that is, M_2XT_x. Each M layer is occupied by two distinct transition metals M′ and M″, where every two atomic rows of M′ are separated by a row of M″ elements (Figure 2a). M′ (the majority M) is typically V, Nb, Cr, Mo, W, and Mn and M″ is typically Sc, Y, Zr. Similar to other MXenes, this unique atomic ordering is derived from their in-plane ordered MAX phase precursors.[47, 48] For example, reactive sintering of an elemental mixture of Mo, Y, Al, and C at 1500 ºC for 20 hours under argon atmosphere results in an in-plane ordered $Mo_{4/3}Y_{2/3}AlC$ MAX phase (Figure 3a).[38] The Al layers are then selectively etched to form in-plane ordered DTM MXenes (Figure 3a-c). The formation of these chemically ordered in-plane structures is primarily attributed to four parameters:[48] i) a 2:1 stoichiometric ratio of M′:M″ elements, ii) significant difference in atomic radii between M′ and M″, where M″ is larger, iii) the large disparity in electronegativities of the M″ elements and the A layer elements, and iv) an A element with small atomic radius.[49] In 2019, in-plane ordered DTM MAX phases with rare earth elements as their M″ were reported. However, their MXenes have not been synthesized yet.[50]

In the in-plane ordered MAX phase precursors, M″ atoms are slightly extended out of the M layers toward the A layers (Figure 3a),[43] which can lead to two different types of MXenes upon selective etching. A milder etching condition, such as shorter etching time or lower hydrogen fluoride (HF) concentration, results in removal of the A layer only and forms $M'_{4/3}M''_{2/3}CT_x$, illustrated by $Mo_{4/3}Y_{2/3}CT_x$ in Figure 3b. The use of stronger etching conditions, for example, longer etching time or higher HF concentration, removes M″ along with the A layers, which forms divacancy ordered MXenes, illustrated by $Mo_{4/3}CT_x$ in Figure 3c.[38] For example, $Mo_{4/3}Y_{2/3}AlC$ MAX phase was etched in 48 wt.% HF at room temperature for 12 and 72 hours to make in-plane ordered DTM $Mo_{4/3}Y_{2/3}CT_x$ and divacancy ordered $Mo_{4/3}CT_x$, respectively.[38] The control of the atomic structure by the presence of ordered rows of M″ versus ordered divacancy creates a unique tool to control the inherent properties, such as electrochemical and electrical conductivity.[38, 46]

When used as an electrode in a supercapacitor, the electrochemical performance of Mo containing in-plane ordered MXenes can be tailored through replacement of in-plane ordered DTM MXenes ($Mo_{4/3}Y_{2/3}CT_x$) to in-plane

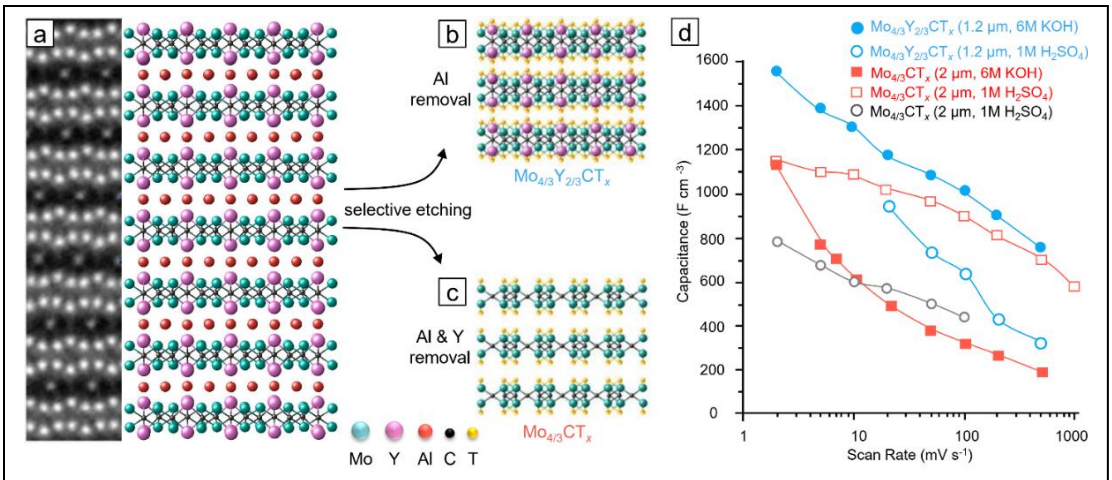

Figure 3. Atomic arrangement of in-plane ordered MXenes and their precursor MAX phase, and their electrochemical performance. (a) Scanning transmission electron microscopy (STEM) image[38] (left) and a schematic (right) of $Mo_{4/3}Y_{2/3}AlC$ MAX phase precursor on [110] axis showing its atomic arrangement. (b) Atomic structure of DTM $Mo_{4/3}Y_{2/3}CT_x$ MXenes after selective etching of aluminum in 48% HF for 12 h. (c) Atomic structure of divacancy $Mo_{4/3}CT_x$ MXenes showing selective etching of both aluminum and in-plane yttrium by longer etching (72 h) in 48% HF. (d) Electrochemical performances of $Mo_{4/3}Y_{2/3}CT_x$ and $Mo_{4/3}CT_x$ in acidic and basic electrolytes showing scan rate and electrolyte dependence of volumetric capacitance. Mono-M Mo_2CT_x MXene is shown for comparison.[38]

divacancy ordered MXenes ($Mo_{4/3}CT_x$). Figure 3d exhibits the volumetric capacitance of these two MXenes synthesized from two in-plane ordered precursors, $Mo_{4/3}Y_{2/3}AlC$ and $Mo_{4/3}Sc_{2/3}AlC$, respectively. It has been shown that $Mo_{4/3}CT_x$ with ordered divacancy exhibits greater volumetric capacitance in acidic electrolytes compared to $Mo_{4/3}Y_{2/3}CT_x$ (open red squares and open blue circles in Figure 3d). However, in a basic electrolyte, the $Mo_{4/3}Y_{2/3}CT_x$ performed better than $Mo_{4/3}CT_x$ (solid blue circles and solid red squares in Figure 3d), which indicates that electrochemical changes also are electrolyte dependent, as shown through the change in MXenes' capacitance from acidic to basic electrolytes in Figure 3d.

The explanation for the change in the electrochemical behavior of these ordered MXenes are not yet fully understood. These changes could be attributed to the increase of electrochemically active sites or the change of surface terminations through the introduction of vacancies and the minority M″.[38] $Mo_{4/3}CT_x$ (with divacancies) has illustrated more –F terminations as compared to Mo_2CT_x.[51] Lower Mo content in $Mo_{4/3}CT_x$ (from 2 to 4/3) leads to the shortage of electrons for surface terminations and results in more –F terminations compared to =O terminations.[51] The higher electrical conductivity of $Mo_{4/3}CT_x$ could also contribute in the in-plane divacancy ordered MXenes' higher electrochemical performace.[46]

Beyond Mo-containing in-plane ordered MXenes, $W_{4/3}CT_x$ MXene is a promising catalyst for hydrogen evolution reaction (HER) activity.[52] However, research in electrochemical and catalytic behavior of in-plane ordered DTM and divacancy MXenes is limited. Studies toward further understanding of the fundamentals of charge transport kinetics in these in-plane ordered DTM MXenes and the effect of vacancies and surface termination compositions on their electrochemical and catalytic performance are necessary to fully realize their potential for various applications.

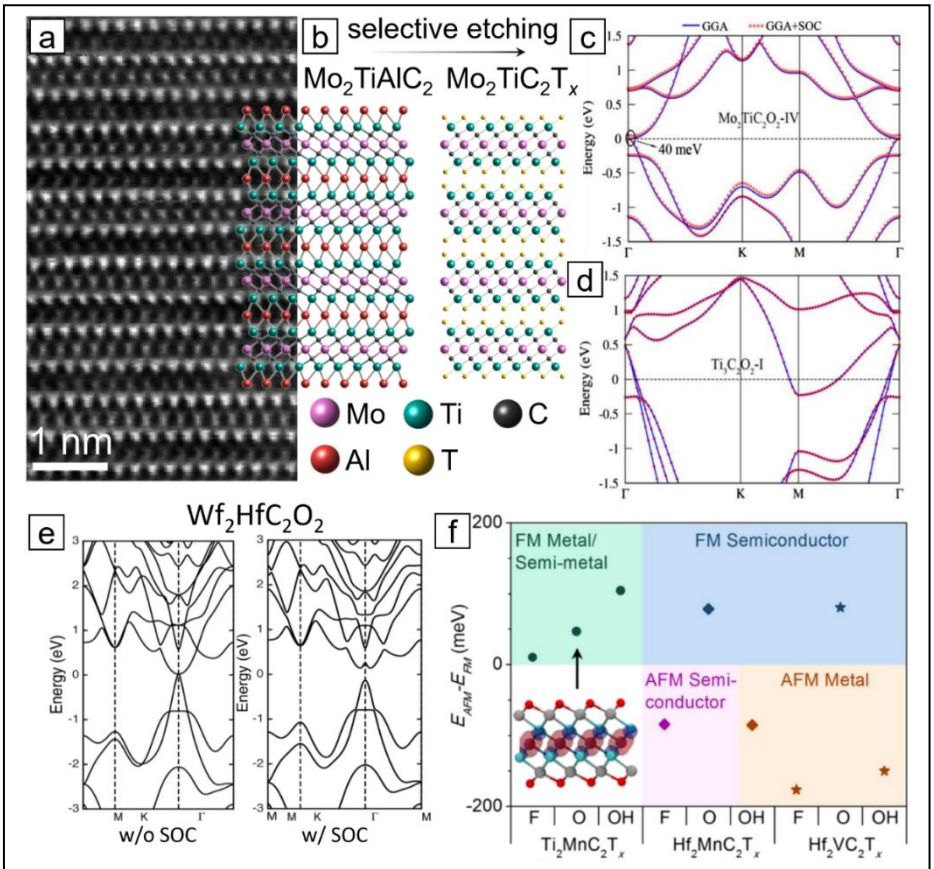

Figure 4. Structure, electronic, and magnetic properties of out-of-plane ordered DTM MXenes. (a) HRSTEM image of Mo_2TiAlC_2 MAX phase.[54] (b) Selective etching process from Mo_2TiAlC_2 to $Mo_2TiC_2T_x$. (c) and (d) Electronic band structure of $Mo_2TiC_2O_2$ and $Ti_3C_2O_2$, respectively, where a slight band gap in semiconducting $Mo_2TiC_2O_2$ is predicted while metallic behavior is predicted in $Ti_3C_2O_2$.[68] (e) The electronic band structure of $W_2HfC_2O_2$, which highlights the band gap induced by accounting for spin-orbit coupling (SOC) of electrons in the *d*-orbital of M′ and M″ in the analysis.[53] (f) Ferromagnetism (FM) and antiferromagnetism (AFM) is seen in theoretical out-of-plane DTM MXenes.[61] Both the M′ and M″ transition metals, as well as the surface terminations, majorly affect the magnetic properties of MXene, where the M′ site determines the interaction with the surface terminations and the M″ site affects the magnitude of magnetic potential.[61]

Out-of-plane ordered double transition metal MXenes

The second type of ordered DTM MXenes, referred to as out-of-plane ordered, are observed in $M_3C_2T_x$ and $M_4C_3T_x$ (Figure 2b). The out-of-plane order refers to the ordering of transition metals in separate atomic planes, in contrast to the in-plane ordered where transition metals are ordered in an atomic plane. In out-of-plane ordered DTM MXenes, inner layers of M″ transition metals (purple atoms in Figure 2b) are sandwiched by outer layers of M′ transition metals (green atoms in Figure 2b) in a layered structure.[37, 53] Like all MXenes, the structural configurations of out-of-plane ordered DTM MXenes begin with synthesis of their precursor MAX phases.[54-56] The only experimentally synthesized out-of-plane ordered DTM MAX phases include Mo_2ScAlC_2,[55] Mo_2TiAlC_2,[54] Cr_2TiAlC_2,[57] Ti_2ZrAlC_2,[58] and $Mo_2Ti_2AlC_3$.[56] Once ordered MAX phases are selectively etched, their derivative MXenes retain the structural ordering of the corresponding MAX phases.[37, 55, 59] From out-of-plane ordered MAX phases, the only synthesized DTM out-of-plane MXenes include $Mo_2ScC_2T_x$,[55] $Mo_2TiC_2T_x$,[37] $Cr_2TiC_2T_x$,[37] and $Mo_2Ti_2C_3T_x$.[37] Figure 4a illustrates a high resolution STEM image of Mo_2TiAlC_2 MAX phase,[54] which is then selectively etched in 48 wt.% HF at 55 ºC for 48 hours to result in $Mo_2TiC_2T_x$ MXene (Figure 4b). Generally, stable

out-of-plane DTM MXenes are predicted to contain Cr, Mo, and W as M′ transition metals and Sc, Ti, Zr, Hf, V, Nb, Ta as M″ transition metals.[60] A complete list of all explored M′ and M″, both experimental and theoretical, is shown in Figure 2b. However, selection of transition metal pairs beyond current experimentally synthesized out-of-plane ordered DTM MXenes will require researchers to prevent disordered solid solutions of these transition metals in their precursor MAX phases, as we discuss later.[42, 60]

The selection of the transition metals pairs in ordered MAX precursors lends considerable control for the electronic, magnetic, optical, and electrochemical properties of their derived ordered out-of-plane DTM MXenes. Significant research is dedicated to the electronic properties of DTM MXenes, with a combination of theoretical[53, 61, 62] and experimental results.[14, 63, 64] In general, the conductivity of mono-M $M_3X_2T_x$ and $M_4X_3T_x$ is metallic, however, some of the out-of-plane ordered DTM MXenes can become semiconductors or semi-metals.[61, 65] Figure 4c and d show DFT simulations of the electronic band structures of semiconducting $Mo_2TiC_2O_2$ (40 meV band gap) and metallic $Ti_3C_2O_2$ with =O surface terminations, respectively.[41] Semiconductor properties in out-of-plane MXenes is due to spin-orbit coupling (SOC) of electrons in the *d*-orbitals between M′ and M″ transition metals[53] or inducing magnetic ordering of an electron into the M′ transition metal *d*-orbital.[66] Both effects are further influenced by interactions of M′ and M″ elements with surface terminations,[53, 66] where a larger difference in electronegativity between transition metals and the surface terminations increases the potential to form semiconductor MXenes.[67] Figure 4e illustrates the effect of SOC of electrons in an out-of-plane DTM MXene, where the consideration of this phenomena changes the prediction of $W_2HfC_2O_2$ from a semi-metal (left panel) to a semiconductor (right panel).[53]

Experimental studies of out-of-plane DTM MXenes have illustrated the surface terminations have the largest effect on the properties of exterior M′ transition metals as compared to the inner M″ transition metals.[69] Therefore, the M′ transition metal and surface terminations in MXenes are important factors to control to form semiconductor MXenes.[41, 53, 61, 70] Theoretical studies predicted M′ transition metals such as Mo, W, Hf, or Cr paired with =O or –F surface terminations to have topological semiconductor band gaps of 0.119 eV, 0.238 eV, 0.409 eV, and 1.26 eV for $Mo_2TiC_2O_2$, $Hf_2MnC_2O_2$, $W_2HfC_2O_2$, and $Cr_2TiC_2F_x$, respectively.[53, 61, 66] However, MXenes with uniform surface functional groups (for example, fully F-terminated) are not yet synthesized, and all synthesized out-of-plane DTM MXenes to date have a mixed of surface terminations and have been electrically conductive.[14, 59, 63, 64, 71] Out-of-plane ordered DTM MXenes are less conductive than $Ti_3C_2T_x$, with the highest film conductivity of 1,490 $S \cdot cm^{-1}$ of $Mo_2Ti_2C_3T_x$ (annealed at ~ 500 ºC) compared to 15,100 $S \cdot cm^{-1}$ of $Ti_3C_2T_x$ (annealed at 200 ºC).[23, 63] Additionally, the conductivity of Mo-containing out-of-plane DTM MXene films is shown to be more dependent on interlayer spacing between MXene flakes due to intercalated molecules used in delamination of out-of-plane DTM MXenes as compared to $Ti_3C_2T_x$.[72]

Similar to the electronic properties, the magnetic behavior of ordered MXenes are controlled by both M′ and M″ elements.[61, 65, 68, 73] To date, M′ = Ti, Hf, Cr and M″ = Mn, V are explored by first-principles methods for magnetic out-of-plane DTM MXenes. Some of these DTM MXenes have been predicted to be ferromagnetic regardless of surface termination, such as $Ti_2MnC_2T_x$ (Figure 4f).[61] Other out-of-plane ordered DTM MXenes are predicted antiferromagnetic, but become ferromagnetic when fully functionalized with =O terminations.[61, 62, 65, 66, 68] The combination of surface terminations with M″ in out-of-plane DTM MXenes affects the electron orbitals in M′, where ferromagnetism in MXenes is based on influencing an electron into a *d*-orbital of the M′ transition metal, which changes the oxidation state from M'^{4+} to M'^{3+}.[53, 61, 66]

Analytical determination of ferromagnetism (FM) versus antiferromagnetism (AFM) can be established by energy difference ($\Delta E = E_{AFM} - E_{FM}$), where positive ΔE represents ferromagnetism and negative ΔE represents antiferromagnetism.[61, 65, 68] Figure 4f illustrates the effect of the composition of both M′ and M″ transition metals, as well as the surface terminations, on the magnetic properties of

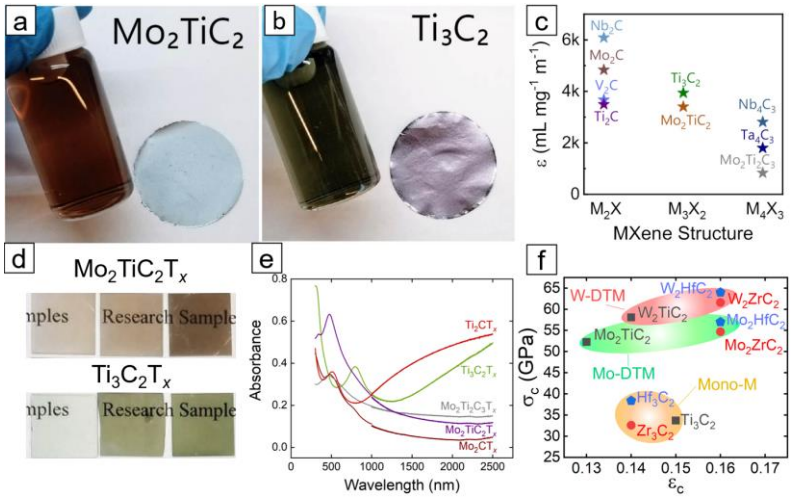

Figure 5. Optical and mechanical properties of out-of-plane ordered DTM MXenes. The color of MXene dispersion and its free-standing film of (a) out-of-plane DTM MXene $Mo_2TiC_2T_x$ and (b) mono-M counterpart $Ti_3C_2T_x$.[74] (c) The extinction coefficient of colloidal dispersions of M_2X, M_3X_2, and M_4X_3 MXenes, which illustrates general trend of lower extinction coefficients of out-of-plane DTM MXenes.[74] (d) Increasing thicknesses (left to right) of spray-coated out-of-plane DTM MXene $Mo_2TiC_2T_x$ and its mono-M counterpart $Ti_3C_2T_x$.[74] (e) The absorbance of thin-films of Mo and Ti mono-M MXenes combined with their out-of-plane ordered DTM MXenes.[74] (f) The improvement effect of M" transition metals on effective ideal strength of $M_3C_2T_x$ (assuming monolayer thickness of $M_3C_2O_2$ as 0.83 nm[76]) vs failure strain as compared to mono-M MXenes.[77] MXenes containing Zr, Hf, and Ti as a mono-M or in a M″ site are denoted by red, blue, and gray markers, respectively. The background ovals highlight either the mono-M MXene range in orange, or Mo or W transition metals in M' sites of DTM MXenes as green or red, respectively.

MXene.[61] Fluorine surface terminations have lower energy toward ferromagnetism for $Ti_2MnC_2F_2$ and $Hf_2MnC_2F_2$ as compared to –OH and =O terminations.[61] However, the tendency for Ti as M'^{3+} and Hf as M'^{4+} in the presence of Mn and –F results in ferromagnetism in $Ti_2MnC_2F_2$ (ΔE = 0.01 eV) and antiferromagnetism in $Hf_2MnC_2F_2$ (ΔE = -0.084 eV).[61] The change of M″ from Mn to V in $Hf_2M''C_2T_x$ affects the magnitude of magnetism, such as $Hf_2VC_2F_2$ (ΔE = -0.177 eV).[61] No ferromagnetic MXenes have been experimentally reported yet due to the difficulty to synthesize a precursor MAX phase (such as $Ti_2MnC_2T_x$), or etch the MAX to form MXene (such as $Cr_2V_2C_3T_x$ [68]).

Next, we turn our attention to the optical properties of out-of-plane DTM MXenes. In general, MXenes in colloidal solutions and thin films of MXenes have different apparent colors depending on their transition metals. Furthermore, the effect of the transition metal in the optical properties is more prominent in thinner MXenes M_2XT_x and $M_3X_2T_x$ as compared to thicker $M_4C_3T_x$ MXenes.[74] In out-of-plane DTM MXenes, such as $M'_2M''C_2T_x$, the optical properties are determined mostly by M'. Figure 5a-b shows the effect of Ti and Mo as the outer M′ layers in a $M_3C_2T_x$ structure on the color of their respective colloidal dispersions and films, while keeping the M″ as Ti in both MXenes.[74] Figure 5c shows colloidal out-of-plane DTM MXenes have lower extinction coefficients (at λ = 200 nm) compared to their mono-M MXene counterparts in both $M_3X_2T_x$ and $M_4X_3T_x$ (for example, 3500 $mg^{-1}mL^{-1}$ in $Mo_2TiC_2T_x$ compared to 4000 $mg^{-1}mL^{-1}$ $Ti_3C_2T_x$).[74] Similar to applications of $Ti_3C_2T_x$ as transparent, highly conductive thin films,[75] semiconductor out-of-plane DTM MXenes, if synthesized, could be used as transparent, semiconductor thin films. Figure 5d shows spray-coated films of a DTM $Mo_2TiC_2T_x$, and a mono-M $Ti_3C_2T_x$ and similarly displays the effect of changing transition metal composition on the color of MXene.[74] Figure 5e highlights the absorbance of spray-coated thin films over a range of wavelengths (at λ = 200 nm to 2500 nm).[74]

Currently, there is no experimental determination of the mechanical properties of DTM MXenes. However, a density functional theory (DFT) study predicted higher effective strengths for out-of-plane ordered DTM MXenes as compared to their mono-M counterparts.[77] In this example, when Mo and W are in M′ sites in $M'_2M''C_2O_2$ (M″: Ti, Zr, Hf) the 2D strengths were increased on average by 60% and 77%, respectively, compared to their mono-M $M_3C_2O_2$ MXenes (M: Ti, Zr, Hf).[77] Figure 5f summarizes the predictions of the strength versus critical strain of ordered out-of-plane DTM MXenes. Although no DFT has been completed on higher order out-of-plane DTM MXenes (e.g., $M'_2M''_2X_3$), increasing thickness (M_3X_2 to M_4X_3) tends to reduce the effective mechanical properties.[76, 78, 79] Nevertheless, MXenes currently rank as the stiffest solution processable nanomaterial,[18, 19] and the improved mechanical properties of out-of-plane ordered DTM MXenes over their mono-M counterparts illustrates the promise for out-of-plane ordered DTM MXenes in this area.

Random solid solution double transition metal MXenes

In contrast with ordered MXenes, solid solution MXenes exhibit random distribution of two different transition metals in M-sites (Figure 2c). While ordered DTM structures are unique to MAX phases and MXenes among all known materials, solid solutions DTM MXenes are similar to solid solutions in other materials, such as bulk carbides and nitrides[80] or other 2D materials, for example,

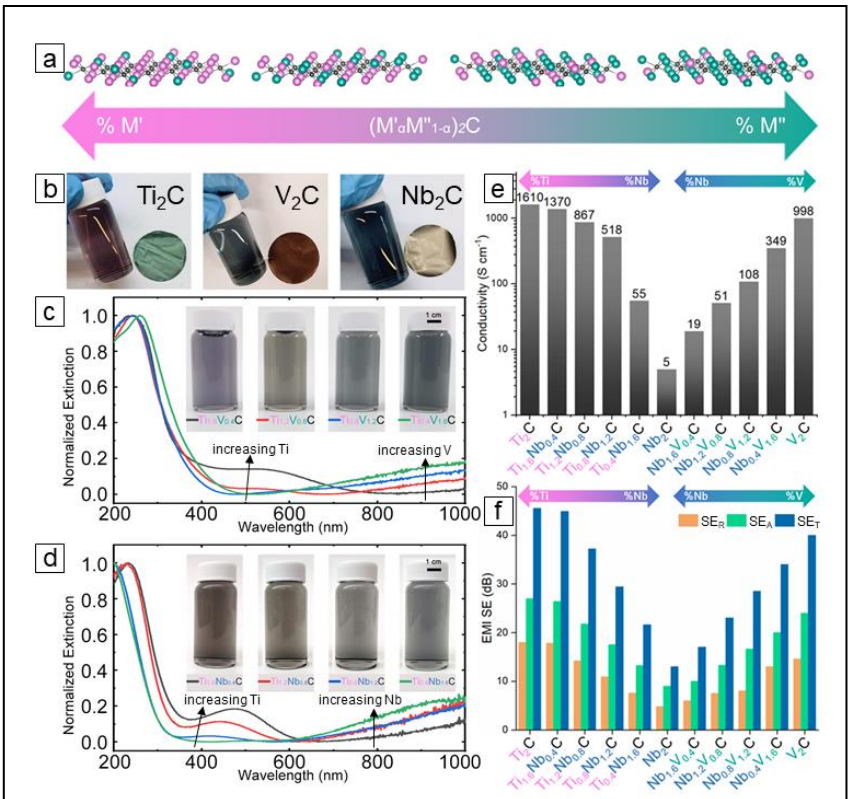

Figure 6. Solid solution MXenes with tunable properties. (a) Schematic representation of the $(M'_\alpha M''_{1-\alpha})_2CT_x$ solid solution MXenes system with various M':M" stoichiometric ratios.[74] T_x is not shown in the schematics for simplicity. (b) The digital images of dispersed mono-M MXenes Ti_2C (left), V_2C (middle), and Nb_2C (right).[74] (c) Digital image and corresponding normalized optical extinction spectra of the $(Ti_\alpha V_{1-\alpha})_2C$ solid solution system changing from Ti-rich sample to V-rich sample.[74] (d) Digital image and corresponding normalized optical extinction spectra of the $(Ti_\alpha Nb_{1-\alpha})_2C$ solid solution system changing from Ti-rich sample to Nb-rich sample.[74] (e) Electrical conductivities of solid solution MXenes by changing their M':M" stoichiometric ratios.[71] (f) The average EMI SE of different MXene films (5 ± 0.3 μm thick) in the 8.2−12.4 GHz range, showing the reflection (SE_R in orange), absorption (SE_A in green) contributions and total SE (SE_T in blue).[71]

transition metal dichalcogenides.[81, 82] The control of stoichiometric ratio of M′ to M″ (M′:M″) provides a continuous control over MXenes' structures and properties. Solid solution MXenes have been reported for all groups of MXenes, M_2CT_x,[45] $M_3C_2T_x$,[40] $M_4C_3T_x$,[39] and even $M_5C_4T_x$.[26] $M_5C_4T_x$ is the highest order of MXenes to date, and has only observed in solid solution MXenes.[26] Unlike ordered MXenes, where only a certain stoichiometric ratio of M′:M″ leads to the formation of ordered MAX phase precursors, solid solution MXenes and their precursor MAX phases encompass a large range of M′:M″. Through control of the stoichiometric ratio of two transition metal in solid solution MXenes, $(M'_\alpha M''_{1-\alpha})_{n+1}C_nT_x$ ($0 < \alpha < 1$), their electrochemical,[39, 44] catalytic,[40] electrical,[71] and optical[74] properties can be tuned between the properties of their two representative mono-M MXenes.

Figure 6a shows schematics of solid solution MXenes as $(M'_\alpha M''_{1-\alpha})_2CT_x$ with different values for α, which changes their M′:M″ ratios. Surface terminations are not shown for simplicity. Figure 6b-d show the control of optical properties by change of the stoichiometric ratio of M′:M″ for two $(M'_\alpha M''_{1-\alpha})_2CT_x$ solid solution phases, $(Ti_\alpha V_{1-\alpha})_2CT_x$, and $(Ti_\alpha Nb_{1-\alpha})_2CT_x$. The optical properties of the colloidal solid solution MXenes (Figure 6c and d) varies between their individual mono-M MXenes (Figure 6b). Both $(Ti,V)_2C$ and $(Ti,Nb)_2C$ show a similar trend in their optical properties, through changes in Ti:V or Ti:Nb ratios. In $(Ti,V)_2C$, the extinction peak position at 550 nm observed in Ti-rich samples is disappeared with increasing V incorporation (Figure 6c). In $(Ti,Nb)_2C$ the extinction peak at around 500 nm shifts to the left (410 nm in $Ti_{0.8}Nb_{1.2}C$) and disappears by further increasing the Nb content (Figure 6d). In both cases, the addition of V or Nb leads to increase in near infrared (above 700 nm) extinction.[74]

Similarly, the electronic conductivity and EMI shielding effectiveness of $(Ti_\alpha Nb_{1-\alpha})_2CT_x$ and $(Nb_\alpha V_{1-\alpha})_2CT_x$ solid solution MXenes can be tuned between Ti_2CT_x and Nb_2CT_x, or Nb_2CT_x and V_2CT_x, respectively, based on their M′:M″ atomic ratio (Figure 6e and f). For example, the electrical conductivity can be tuned between 5 to 1,610 $S \cdot cm^{-1}$ through variation of α from 0 to 1 in $(Ti_\alpha Nb_{1-\alpha})_2CT_x$.[71] This is similarly seen in thicker MXenes such as in $M_4X_3T_x$ structures. For example, in $(Mo_\alpha V_{1-\alpha})_4C_3T_x$ solid solution MXenes, electrical conductivity shows more than an order of magnitude increase from 15 $S.cm^{-1}$ for $(MoV_3)C_3T_x$ ($\alpha = 0.25$) to 830 $S.cm^{-1}$ for $(Mo_{2.7}V_{1.3})C_3T_x$ ($\alpha = 0.675$).[44] This control of properties by changing the M′:M″ ratios shows the potential of solid solution MXenes in application-driven design.

Similar to ordered MXenes, the control of stoichiometry in solid solution MXenes comes from their MAX phase precursors. Although solid solution MXenes have been reported as early as 2012,[11] and more than thousands of predicted compositions of solid solutions,[83] there are a very limited number of studies on solid solution MXenes (Figure 2c). Additionally, many solid solution MAX phases, such as $(Cr_\alpha Mn_{1-\alpha})_2AlC$, have not yet been etched to MXene.[84] All experimentally reported solid solution DTM MAX phases that their MXenes are not made yet are marked with horizontal striped background in Figure 2c.

Parameters controlling ordered and solid solution MXene formations

The formation criteria of both ordered MXenes and solid solution MXenes is necessary to understand the preferred structure of DTM MXenes as solid solutions or ordered transition metals. The M ordering of MXenes is dependent on total energy or formation energy, which is changed by the choice of transition metal pairs.[37, 42] Figure 7a shows the total energy diagram of a selection of $M'_2M''_2C_3$ DTM MXenes with different configurations varied from fully ordered (left) to solid solutions (right).[37] For these specific selection of transition metal pairs, fully ordered DTM MXene (100 % M″ in the middle layers) illustrate lower theoretical total energies as compared to disordered solid solution configurations, which indicates that ordered configurations are more stable at 0 K.[37]

However, the degree of favorability for ordered versus solid solution DTM MXene structures depends on the transition metals pairs. For example, in $Mo_2Ti_2C_3T_x$ MXene, the change of Mo/Ti occupancy in the four M layers from ordered to solid solution increases the formation energy by ~ 0.5 eV (Figure 7a). Due to this large difference in formation energy between ordered and disordered Mo-Ti DTM MXenes, $Mo_2Ti_2C_3T_x$ has been synthesized and characterized only as an ordered DTM MXene.[37] In contrast, for a Mo-V-containing DTM MXene $M_4C_3T_x$, the change of formation energy from ordered to solid solution is among the smallest (~0.2 eV) as shown Figure 7a. Due to the high heats required to form MAX phases (>1700 K), we speculate that the small difference in formation energy between ordered and solid solutions is overcome by the increased effect of entropy by the high thermal energy needed for MAX formation,[42] which results in preference for the transition metal pair Mo-V to form solid solutions. The effect of high heats for formation of precursor MAX phases has been illustrated experimentally, as all formed Mo-V DTM MXenes to date have been found in solid solution $(Mo_\alpha V_{1-\alpha})_4C_3T_x$ configurations.[44]

X-ray diffraction (XRD) can be used to determine which atomic arrangement (ordered versus solid solution) forms in the DTM MAX phase precursors. When a solid solution is formed, changing the M′:M″ stoichiometric ratios result in similar XRD patterns with slightly shifted peaks, due to slight changes in the lattice parameters. For example, by changing the Mo:V ratio in the $(Mo_\alpha V_{1-\alpha})_4AlC_3$ solid solution, peak shifting was observed due to the solid solution effect (Figure 7b and 7c).[44] By increasing the V element content, the (002) peak of $(Mo_\alpha V_{1-\alpha})_4AlC_3$ shifted to higher angles (Figure 7c). In contrast, when ordered DTM MAX phases are formed, changing the M′:M″ ratios gives different XRD spectra indicating different phase formation. For example, the XRD patterns of three Mo:Ti ratios of 2.7:1.3, 2.5:1.5, and 2:2 are shown in Figure 7d. All three

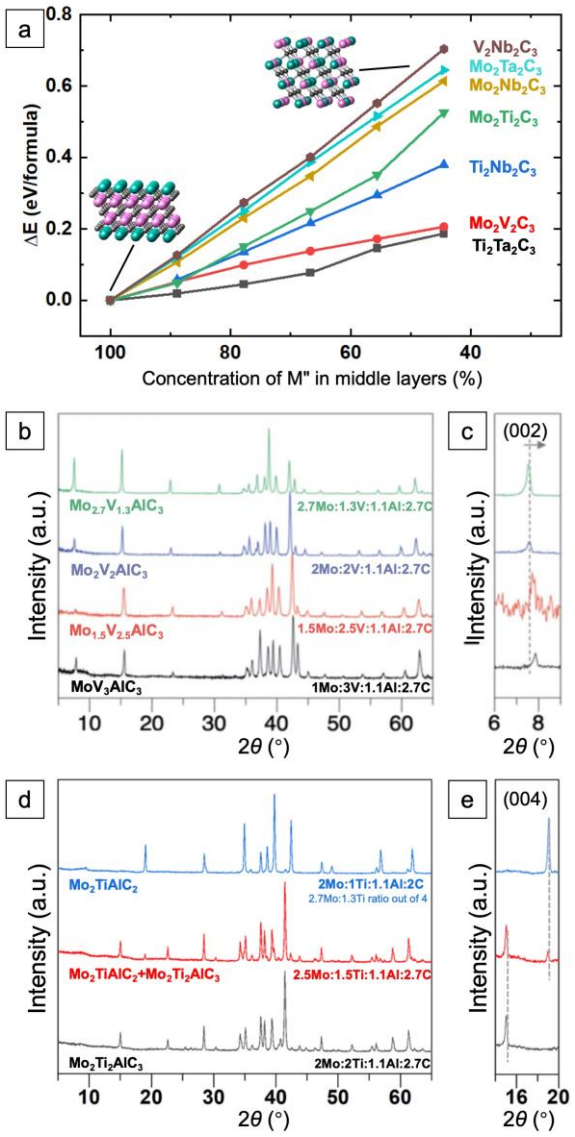

Figure 7. Predicted stability of DTM MXenes and XRD patterns of DTM MAX phases. (a) Total energy diagrams of calculated M'$_2$M"$_2$C$_3$ MXene with respect to concentration of M" in the middle layers.[37] Predictions of MXene stabilities were conducted at 0 K. (b) XRD patterns of $(Mo_\alpha V_{1-\alpha})_4AlC_3$ MAX phases. (c) Close view of (002) peaks shift to right by increasing V content. (d) XRD patterns of ordered Mo_2TiAlC_2 and $Mo_2Ti_2AlC_3$ MAX phases. (e) Close view of (004) peaks, showing not following the stoichiometric ratio leads to formation of both Mo_2TiAlC_2 and $Mo_2Ti_2AlC_3$ MAX phases mixture (middle pattern).

ratios were sintered at similar conditions. However, each leads to either ordered M_3AlC_2 for Mo:Ti 2.7:1.3 (top pattern in Figure 7d) or ordered M_4AlC_3 for Mo:Ti 2:2 ratio (bottom pattern in Figure 7d). The (004) peaks in their XRD patterns (Figure 7e) clearly show that not following the stoichiometric ratio (for example, Mo:Ti = 2.5:1.5) leads to a mixture containing two ordered MAX phases without any peaks shifting.[56] According to recent theoretical study of DTM MAX, out-of-plane ordered structures are predicted to form out of combinations of M′ and M″ which have a large difference in electronegativity (>0.4), an increased difference in atomic radii (0.2 Å), as well as an increased difference in electronegativity between M′ and the A-group element in the MAX phase precursor.[60] Combinations of transition metal pairs which do not follow these general trends for ordered DTM MAX formation tend to form solid solution structures.[60] Based on these general trends, solid solution structures are more likely in phases comprised of transition metal pairs from groups 3-5 of the periodic table (Sc, Ti, V, Zr, Nb, Hf, Ta).[60]

Future Scope and outlook

Double transition metal MXenes are in their early stages of research and development since there are many compositions yet to be explored experimentally or computationally. Although more than fifty ordered DTM compositions are theoretically stable in both MAX phases and MXenes, only ten have been experimentally realized (Figure 2a and 2b). Even in computational research, the properties and structures of very few ordered DTM MXenes have been investigated. With the addition of solid solution DTM MXenes, the number of composition possibilities and potential for tunable properties becomes limitless, which opens new approaches to the design of 2D materials with fine-tuned properties for specific applications. Exploration of the effect of transition metals on properties of MXenes by theoretical methods can give guidance for future studies on theory-guided-synthesis of new MXenes.

The number of possibilities for DTM MXenes increases with the consideration of recent scientific advances made in MAX phase precursors. Currently, there are ordered and solid solution DTM MAX phases which have been synthesized, but not yet etched to their respective DTM MXenes (marked with horizontal striped background in Figure 2). Additionally, current research has only discussed DTM MXenes made from carbide MAX phases, and no nitride or carbonitride DTM MXenes have been explored, although some mono-M nitride[85] and carbonitride[86] MXenes have been experimentally realized. As nitride and carbonitride MXenes have illustrated different properties than their carbide counterparts in energy storage applications,[87-89] it is expected that nitrogen or carbon/nitrogen as X in MXene will affect the properties of potential DTM nitride/carbonitride MXenes. Computational studies should investigate the use of nitrogen or carbon/nitrogen as X in DTM MXenes and their effects on MXenes structures and properties.

The possibilities for DTM MXenes can be further increased with the addition of tunable surface terminations. Full control over MXenes' termination compositions is yet to be experimentally realized despite DFT studies suggesting unique properties, such as magnetic [61] or topological insulation.[53] With the consideration of surface terminations, the control of the ratio of transition metal pairs in solid solutions, and the addition of DTM MXene nitrides

or carbonitrides, the number of possible DTM MXene compositions becomes limitless.

Additionally, all DTM MXenes have been made from aluminum-containing MAX phases to date.[43] Recently, new methods of selective etching show that MXenes from non-Al-based MAX phases can be successfully synthesized.[35, 90] The use of A-group elements with different electronegativities could allow formation of in-plane, out-of-plane, or solid solution DTM MAX phases comprised of transition metal pairs which do not form these structures when Al is used as the A-group element. Additionally, etching of other A-group elements allows the synthesis of Mn-containing MXenes from already available Mn-containing MAX phases.[84, 91] Moreover, in 2019, the family of in-plane ordered DTM MAX phases expanded to include rare-earth elements, such as Ce, Pr, Nd, Sm, Gd, Tb, Dy, Ho, Er, Tm, and Lu.[50] If rare-earth MXenes can be realized through controlled etching conditions, it opens door to *f*-block element MXenes. This could lead to novel behavior which has not yet been identified in MXenes. MXenes which contain three or more transition metals (multi-principal element MXenes) have not yet been explored computationally or experimentally yet, which can expand MXenes towards high entropy 2D materials. The addition of more complexity in MXene compositions could give new means of controlling properties.

Summary

The family of MXenes has now expanded to include in-plane ordered, out-of-plane ordered, and disordered DTM MXenes. This review has summarized the general rules of formation of each DTM MXene structure and their tunable properties based on transition metal composition. All three types of DTM MXenes have illustrated behavior not yet seen in mono-M MXenes, which indicates promise for the use of DTM MXenes in a variety of novel applications. As we have identified, the control of the composition of DTM MXenes' precursor MAX phase allows researchers to tune the performance of MXenes for a range of applications, from supercapacitors, semiconductors, transparent electronics, nano-magnets, and structural materials. The addition of DTM MXenes to family of 2D materials has expanded the design scope of nanomaterials to meet the demands of an evolving technological sphere.

References

1. X. Zhang, L. Hou, A. Ciesielski, P. Samorì, *Adv. Energy Mater.* **6**, 1600671 (2016).
2. E. Pomerantseva, Y. Gogotsi, *Nat. Energy.* **2**, 1 (2017).
3. B. Xu, S. Qi, M. Jin, X. Cai, L. Lai, Z. Sun, X. Han, Z. Lin, H. Shao, P. Peng, *Chin. Chem. Lett.* **30**, 2053 (2019).
4. H. Kim, H. N. Alshareef, *ACS Mater. Lett.* **2**, 55 (2019).
5. L. Ding, Y. Wei, Y. Wang, H. Chen, J. Caro, H. Wang, *Angew. Chem. Int. Ed.* **56**, 1825 (2017).
6. P. Sun, M. Zhu, K. Wang, M. Zhong, J. Wei, D. Wu, Z. Xu, H. Zhu, *ACS Nano.* **7**, 428 (2013).
7. T. Y. Ma, J. L. Cao, M. Jaroniec, S. Z. Qiao, *Angew. Chem. Int. Ed.* **55**, 1138 (2016).
8. W. Yuan, G. Shi, *J. Mater. Chem. A.* **1**, 10078 (2013).
9. W. Yang, K. R. Ratinac, S. P. Ringer, P. Thordarson, J. J. Gooding, F. Braet, *Angew. Chem. Int. Ed.* **49**, 2114 (2010).
10. M. Naguib, M. Kurtoglu, V. Presser, J. Lu, J. Niu, M. Heon, L. Hultman, Y. Gogotsi, M. W. Barsoum, *Adv. Mater.* **23**, 4248 (2011).
11. M. Naguib, O. Mashtalir, J. Carle, V. Presser, J. Lu, L. Hultman, Y. Gogotsi, M. W. Barsoum, *ACS Nano.* **6**, 1322 (2012).
12. M. Khazaei, M. Arai, T. Sasaki, C.-Y. Chung, N. S. Venkataramanan, M. Estili, Y. Sakka, Y. Kawazoe, *Adv. Funct. Mater.* **23**, 2185 (2013).
13. M. Khazaei, A. Ranjbar, M. Arai, T. Sasaki, S. Yunoki, *J. Mater. Chem. C.* **5**, 2488 (2017).
14. B. Anasori, C. Shi, E. J. Moon, Y. Xie, C. A. Voigt, P. R. Kent, S. J. May, S. J. Billinge, M. W. Barsoum, Y. Gogotsi, *Nanoscale Horiz.* **1**, 227 (2016).
15. K. Hantanasirisakul, M. Q. Zhao, P. Urbankowski, J. Halim, B. Anasori, S. Kota, C. E. Ren, M. W. Barsoum, Y. Gogotsi, *Adv. Electron. Mater.* **2**, 1600050 (2016).
16. H. Zhang, G. Yang, X. Zuo, H. Tang, Q. Yang, G. Li, *J. Mater. Chem. A.* **4**, 12913 (2016).
17. A. D. Dillon, M. J. Ghidiu, A. L. Krick, J. Griggs, S. J. May, Y. Gogotsi, M. W. Barsoum, A. T. Fafarman, *Adv. Funct. Mater.* **26**, 4162 (2016).
18. A. Lipatov, H. Lu, M. Alhabeb, B. Anasori, A. Gruverman, Y. Gogotsi, A. Sinitskii, *Sci. Adv.* **4**, eaat0491 (2018).
19. A. Lipatov, M. Alhabeb, H. Lu, S. Zhao, M. J. Loes, N. S. Vorobeva, Y. Dall'Agnese, Y. Gao, A. Gruverman, Y. Gogotsi, *Adv. Electron. Mater.* **6**, 1901382 (2020).
20. X.-H. Zha, K. Luo, Q. Li, Q. Huang, J. He, X. Wen, S. Du, *EPL.* **111**, 26007 (2015).
21. M. Alhabeb, K. Maleski, B. Anasori, P. Lelyukh, L. Clark, S. Sin, Y. Gogotsi, *Chem. Mater.* **29**, 7633 (2017).
22. K. Maleski, V. N. Mochalin, Y. Gogotsi, *Chem. Mater.* **29**, 1632 (2017).
23. J. Zhang, N. Kong, S. Uzun, A. Levitt, S. Seyedin, P. A. Lynch, S. Qin, M. Han, W. Yang, J. Liu, *Adv. Mater.* **32**, 2001093 (2020).
24. F. Shahzad, M. Alhabeb, C. B. Hatter, B. Anasori, S. M. Hong, C. M. Koo, Y. Gogotsi, *Science.* **353**, 1137 (2016).
25. B. Anasori, M. R. Lukatskaya, Y. Gogotsi, *Nat. Rev. Mater.* **2**, 16098 (2017).
26. G. Deysher, C. E. Shuck, K. Hantanasirisakul, N. C. Frey, A. C. Foucher, K. Maleski, A. Sarycheva, V. B. Shenoy, E. A. Stach, B. Anasori, *ACS Nano.* **14**, 204 (2020).
27. M. Naguib, V. N. Mochalin, M. W. Barsoum, Y. Gogotsi, *Adv. Mater.* **26**, 992 (2014).
28. Y. Gogotsi, B. Anasori, *ACS Nano.* **13**, 8491 (2019).
29. M. Radovic, M. W. Barsoum, *Am. Ceram. Soc. Bull.* **92**, 20 (2013).
30. J. Zhou, X. Zha, F. Y. Chen, Q. Ye, P. Eklund, S. Du, Q. Huang, *Angew. Chem. Int. Ed.* **55**, 5008 (2016).
31. M. Sokol, V. Natu, S. Kota, M. W. Barsoum, *Trends Chem.* **1**, 210 (2019).
32. M. Khazaei, A. Ranjbar, K. Esfarjani, D. Bogdanovski, R. Dronskowski, S. Yunoki, *Phys. Chem. Chem. Phys.* **20**, 8579 (2018).
33. M. A. Hope, A. C. Forse, K. J. Griffith, M. R. Lukatskaya, M. Ghidiu, Y. Gogotsi, C. P. Grey, *Phys. Chem. Chem. Phys.* **18**, 5099 (2016).

34. X. Wang, X. Shen, Y. Gao, Z. Wang, R. Yu, L. Chen, *J. Am. Chem. Soc.* **137**, 2715 (2015).
35. Y. Li, H. Shao, Z. Lin, J. Lu, L. Liu, B. Duployer, P. O. Persson, P. Eklund, L. Hultman, M. Li, *Nat. Mater.*, 1 (2020).
36. I. Persson, L.-Å. Näslund, J. Halim, M. W. Barsoum, V. Darakchieva, J. Palisaitis, J. Rosen, P. O. Å. Persson, *2D Mater.* **5**, 015002 (2017).
37. B. Anasori, Y. Xie, M. Beidaghi, J. Lu, B. C. Hosler, L. Hultman, P. R. C. Kent, Y. Gogotsi, M. W. Barsoum, *ACS Nano.* **9**, 9507 (2015).
38. I. Persson, A. el Ghazaly, Q. Tao, J. Halim, S. Kota, V. Darakchieva, J. Palisaitis, M. W. Barsoum, J. Rosen, P. O. A. Persson, *Small* **14**, 1703676 (2018).
39. J. Yang, M. Naguib, M. Ghidiu, L. M. Pan, J. Gu, J. Nanda, J. Halim, Y. Gogotsi, M. W. Barsoum, *J. Am. Ceram. Soc.* **99**, 660 (2016).
40. Z. Shen, Z. Wang, M. Zhang, M. Gao, J. Hu, F. Du, Y. Liu, H. Pan, *Materialia.* **1**, 114 (2018).
41. L. Li, *Comput. Mater. Sci.* **124**, 8 (2016).
42. T. L. Tan, H. M. Jin, M. B. Sullivan, B. Anasori, Y. Gogotsi, *ACS Nano.* **11**, 4407 (2017).
43. J. Rosen, M. Dahlqvist, Q. Tao, L. Hultman, in *2D Metal Carbides and Nitrides (MXenes)*. (Springer, 2019), pp. 37-52.
44. D. Pinto, B. Anasori, H. Avireddy, C. E. Shuck, K. Hantanasirisakul, G. Deysher, J. R. Morante, W. Porzio, H. N. Alshareef, Y. Gogotsi, *J. Mater. Chem. A.* **8**, 8957 (2020).
45. S. Yazdanparast, S. Soltanmohammad, A. Fash-White, G. Tucker, G. L. Brennecka, *ACS Appl. Mater. Interfaces.* **12**, 20129 (2020).
46. Q. Tao, M. Dahlqvist, J. Lu, S. Kota, R. Meshkian, J. Halim, J. Palisaitis, L. Hultman, M. W. Barsoum, P. O. Persson, *Nat. Commun.* **8**, 14949 (2017).
47. L. Chen, M. Dahlqvist, T. Lapauw, B. Tunca, F. Wang, J. Lu, R. Meshkian, K. Lambrinou, B. Blanpain, J. Vleugels, *Inorg. Chem.* **57**, 6237 (2018).
48. M. Dahlqvist, J. Lu, R. Meshkian, Q. Tao, L. Hultman, J. Rosen, *Sci. Adv.* **3**, e1700642 (2017).
49. M. Dahlqvist, A. Petruhins, J. Lu, L. Hultman, J. Rosen, *ACS Nano.* **12**, 7761 (2018).
50. Q. Tao, J. Lu, M. Dahlqvist, A. Mockute, S. Calder, A. Petruhins, R. Meshkian, O. Rivin, D. Potashnikov, E. a. N. Caspi, H. Shaked, A. Hoser, C. Opagiste, R.-M. Galera, R. Salikhov, U. Wiedwald, C. Ritter, A. R. Wildes, B. Johansson, L. Hultman, M. Farle, M. W. Barsoum, J. Rosen, *Chem. Mater.* **31**, 2476 (2019).
51. H. Lind, J. Halim, S. Simak, J. Rosén, *Phys. Rev. Mater.* **1**, 044002 (2017).
52. R. Meshkian, M. Dahlqvist, J. Lu, B. Wickman, J. Halim, J. Thornberg, Q. Tao, S. Li, S. Intikhab, J. Snyder, M. W. Barsoum, M. Yildizhan, J. Palisaitis, L. Hultman, P. O. A. Persson, J. Rosen, *Adv. Mater.* **30**, 1706409 (2018).
53. M. Khazaei, A. Ranjbar, M. Arai, S. Yunoki, *Phys. Rev. B.* **94**, 125152 (2016).
54. B. Anasori, J. Halim, J. Lu, C. A. Voigt, L. Hultman, M. W. Barsoum, *Scr. Mater.* **101**, 5 (2015).
55. R. Meshkian, Q. Tao, M. Dahlqvist, J. Lu, L. Hultman, J. Rosen, *Acta Mater.* **125**, 476 (2017).
56. B. Anasori, M. Dahlqvist, J. Halim, E. J. Moon, J. Lu, B. C. Hosler, E. a. N. Caspi, S. J. May, L. Hultman, P. Eklund, *J. Appl. Phys.* **118**, 094304 (2015).
57. Z. Liu, L. Zheng, L. Sun, Y. Qian, J. Wang, M. Li, *J. Am. Ceram. Soc.* **97**, 67 (2014).
58. B. Tunca, T. Lapauw, O. M. Karakulina, M. Batuk, T. Cabioc'h, J. Hadermann, R. m. Delville, K. Lambrinou, J. Vleugels, *Inorg. Chem.* **56**, 3489 (2017).
59. G. Lui, V. Natu, T. Shi, M. W. Barsoum, L. V. Titova, *ACS Appl. Energy Mater.* **3**, 1530 (2020).
60. M. Dahlqvist, J. Rosen, *Nanoscale* **12**, 785 (2020).
61. L. Dong, H. Kumar, B. Anasori, Y. Gogotsi, V. B. Shenoy, *J. Phys. Chem. Lett.* **8**, 422 (2017).
62. W. W. Sun, Y. Xie, P. R. C. Kent, *Nanoscale* **10**, 11962 (2018).
63. H. Kim, B. Anasori, Y. Gogotsi, H. N. Alshareef, *Chem. Mater.* **29**, 6472 (2017).
64. J. L. Hart, K. Hantanasirisakul, A. C. Lang, B. Anasori, D. Pinto, Y. Pivak, J. T. van Omme, S. J. May, Y. Gogotsi, M. L. Taheri, *Nat. Commun.* **10**, 1 (2019).
65. E. M. D. Siriwardane, D. Cakir, *J. Appl. Phys.* **125**, 082527 (2019).
66. J. J. He, G. Q. Ding, C. Y. Zhong, S. Li, D. F. Li, G. Zhang, *Nanoscale* **11**, 356 (2019).
67. A. C. Rajan, A. Mishra, S. Satsangi, R. Vaish, H. Mizuseki, K.-R. Lee, A. K. Singh, *Chem. Mater.* **30**, 4031 (2018).
68. J. H. Yang, X. P. Luo, X. M. Zhou, S. Z. Zhang, J. Liu, Y. Xie, L. Lv, L. Chen, *Comput. Mater. Sci.* **139**, 313 (2017).
69. Y. Yang, K. Hantanasirisakul, N. Frey, B. Anasori, R. Green, P. Rogge, I. Waluyo, A. Hunt, P. Shafer, E. Arenholz, *2D Mater.* **7**, 025015 (2020).
70. Z. H. Fu, Z. R. Liu, D. Legut, T. C. Germann, C. Si, S. Y. Du, J. S. Francisco, R. F. Zhang, *J. Phys. Chem. C* **123**, 20664 (2019).
71. M. Han, C. E. Shuck, R. Rakhmanov, D. Parchment, B. Anasori, C. M. Koo, G. Friedman, Y. Gogotsi, *ACS Nano.* **14**, 5008 (2020).
72. J. Halim, E. J. Moon, P. Eklund, J. Rosen, M. W. Barsoum, T. Ouisse, *Phys. Rev. B.* **98**, 104202 (2018).
73. Y. Hu, X. Fan, W. Guo, Y. An, Z. Luo, J. Kong, *J. Magn. Magn. Mater.* **486**, 165280 (2019).
74. K. Maleski, *Drexel University Ph.D. Desertation*, (2020).
75. C. Zhang, B. Anasori, A. Seral-Ascaso, S. H. Park, N. McEvoy, A. Shmeliov, G. S. Duesberg, J. N. Coleman, Y. Gogotsi, V. Nicolosi, *Adv. Mater.* **29**, 1702678 (2017).
76. G. Plummer, B. Anasori, Y. Gogotsi, G. J. Tucker, *Comput. Mater. Sci.* **157**, 168 (2019).
77. Z. H. Fu, S. H. Zhang, D. Legut, T. C. Germann, C. Si, S. Y. Du, J. S. Francisco, R. F. Zhang, *Phys. Chem. Chem. Phys.* **20**, 29684 (2018).
78. M. Kurtoglu, M. Naguib, Y. Gogotsi, M. W. Barsoum, *MRS Commun.* **2**, 133 (2012).
79. V. N. Borysiuk, V. N. Mochalin, Y. Gogotsi, *Nanotechnology.* **26**, 265705 (2015).
80. E. Rudy, "Ternary phase equilibria in transition metal-boron-carbon-silicon systems. part 5. compendium of phase diagram data," (Aerojet-general corp sacramento ca materials research lab 1969).
81. H. Wang, H. Yuan, S. S. Hong, Y. Li, Y. Cui, *Chem. Soc. Rev.* **44**, 2664 (2015).
82. Y. Chen, J. Xi, D. O. Dumcenco, Z. Liu, K. Suenaga, D. Wang, Z. Shuai, Y.-S. Huang, L. Xie, *ACS Nano.* **7**, 4610 (2013).
83. M. Ashton, R. G. Hennig, S. R. Broderick, K. Rajan, S. B. Sinnott, *Phys. Rev. B.* **94**, 054116 (2016).
84. A. S. Ingason, M. Dahlqvist, J. Rosén, *J. Phys.: Condens. Matter* **28**, 433003 (2016).

85. P. Urbankowski, B. Anasori, T. Makaryan, D. Er, S. Kota, P. L. Walsh, M. Zhao, V. B. Shenoy, M. W. Barsoum, Y. Gogotsi, *Nanoscale* **8**, 11385 (2016).
86. K. Hantanasirisakul, M. Alhabeb, A. Lipatov, K. Maleski, B. Anasori, P. Salles, C. Ieosakulrat, P. Pakawatpanurut, A. Sinitskii, S. J. May, *Chem. Mater.* **31**, 2941 (2019).
87. X. Liang, Y. Rangom, C. Y. Kwok, Q. Pang, L. F. Nazar, *Adv. Mater.* **29**, 1603040 (2017).
88. X. Tang, X. Guo, W. Wu, G. Wang, *Adv. Energy Mater.* **8**, 1801897 (2018).
89. H. Lin, D.-D. Yang, N. Lou, S.-G. Zhu, H.-Z. Li, *Ceram. Int.* **45**, 1588 (2019).
90. M. Li, J. Lu, K. Luo, Y. Li, K. Chang, K. Chen, J. Zhou, J. Rosen, L. Hultman, P. Eklund, P. O. Å. Persson, S. Du, Z. Chai, Z. Huang, Q. Huang, *J. Am. Chem. Soc.* **141**, 4730 (2019).
91. A. Mockuté, J. Lu, E. Moon, M. Yan, B. Anasori, S. May, M. Barsoum, J. Rosén, *Mater. Res. Lett.* **3**, 16 (2015).

. . . . . .

Weichen Hong is a first year PhD student and a research assistant in the layered materials and structures lab at the department of mechanical and energy engineering, IUPUI, Indianapolis. He joined Dr. Anasori's research group in Fall 2019. He received his BS and MS in material science engineering from the Wuhan University of Technology in 2017 and 2019, respectively. His research interests include new MAX phases exploration and corresponding MXenes' synthesis, characterization, and applications for energy storage and electronics. Hong can be reached by email at hweichen@purdue.edu.

. . . . . .

Brian Cecil Wyatt is a first year PhD student in the layered materials and structures lab in the Mechanical and Energy Engineering department at Indiana University – Purdue University – Indianapolis. He received his Bachelor of Science degree in Mechanical Engineering at Rose-Hulman Institute of Technology in Terre Haute, IN in 2019. His current research focus is on the inclusion of MXenes into lightweight metals for bio-inspired structural application. His scientific interests include the mechanical characterization and composition control of two-dimensional nanomaterials as well as the investigation of their interfacial properties in structural composite materials. Brian can be reached by email at bcwyatt@iu.edu.

. . . . . .

Srinivasa Kartik Nemani is a first year PhD student and a research assistant in the layered materials and structures lab at the department of mechanical and energy engineering, IUPUI, Indianapolis. He joined Dr. Anasori's research group in Fall 2019. He received his MS in mechanical engineering from the University of Toledo in 2018. His current scientific interests are in the field of MXenes, composites, and hybrid materials where he is working on synthesizing MXenes and developing MXene reinforced materials for various applications. He has published articles in several journals including advanced materials interfaces, and ACS applied materials & interfaces. Kartik can be reached by email at snemani@purdue.edu.

. . . . . .

Babak Anasori is an Assistant Professor at Purdue School of Engineering and Technology in IUPUI. He received his PhD at Drexel University in 2014 in Materials Science and Engineering. Babak is one of the inventors of ordered double-transition metal MXenes, as a result of his postdoctoral research. His current research focuses on the synthesis and characterizations of novel MXenes and their composites. He has co-authored over 120 journal papers, most of them on MXenes. Babak co-edited the first book on MXenes in 2019, and he is among the Global Highly Cited Researchers 2019 recognized by the Web of Science. He is currently the chair of the Early Career Professionals Subcommittee of MRS. Anasori can be reached by email at banasori@iupui.edu.